Design Method for Circularly Polarized Fabry-Perot Cavity Antennas

Orr, R., Goussetis, G., & Fusco, V. (2014). Design Method for Circularly Polarized Fabry-Perot Cavity Antennas. *IEEE Transactions on Antennas and Propagation*, *62*(1), 19-26. [6644269]. https://doi.org/10.1109/TAP.2013.2286839

Published in:
IEEE Transactions on Antennas and Propagation

Document Version:
Peer reviewed version

This article has been accepted for publication in a future issue of this journal, but has not been fully edited. Content may change prior to final publication. Citation information: DOI 10.1109/TAP.2013.2286839, IEEE Transactions on Antennas and Propagation

Design Method for Circularly Polarized Fabry-Perot Cavity Antennas

Robert Orr, George Goussetis, *Senior Member, IEEE,* and Vincent Fusco*, Fellow, IEEE*

***Abstract*—A new class of circularly polarized (CP) Fabry-Perot cavity antennas is introduced that maintain the simplicity of a linearly polarized primary feed and a single cavity structure. The proposed antennas employ a double-sided partially reflective surface (PRS), which allows independent control of the magnitude and phase responses for the reflection and transmission coefficients. In conjunction with an anisotropic high impedance surface (HIS) ground plane, this arrangement allows for the first time a single cavity antenna to produce a specified gain in CP from a linearly polarized primary source. A design procedure for this class of antennas is introduced. The method exploits a simple ray optics model to calculate the magnitude and phase of the electric field in the cavity upon plane wave excitation. Based on this model, analytical expressions are derived, which enforce the resonance condition for both polarizations at a predetermined PRS reflectivity (and hence predetermined antenna gain) together with a 90° differential phase between them. The validity of the concept is confirmed by means of an example entailing an antenna with gain of approximately 21 dB at 15 GHz. Full-wave simulation results and experimental testing on a fabricated prototype are presented and agree well with the theoretical predictions.**

***Index Terms*—Directive antenna, partially reflective surface, resonant cavity antenna, high impedance surface.**

I. Introduction

FABRY-PEROT (FP) antennas have been identified as an attractive high gain antenna solution due to their low profile and mass as well as fabrication simplicity and cost-saving potential when compared with bulky horns or corporate-fed arrays [1]-[8]. They typically comprise a simple linearly polarized (LP) source, such as a dipole or printed patch, placed in the cavity formed between a partially reflecting surface (PRS) and a fully reflective ground plane. Directive LP emission is achieved upon establishing a Fabry-Perot type resonance within the cavity. The resonant characteristics of the cavity, which in turn can be tailored by the properties of the PRS and the full reflector, will primarily determine antenna performance.

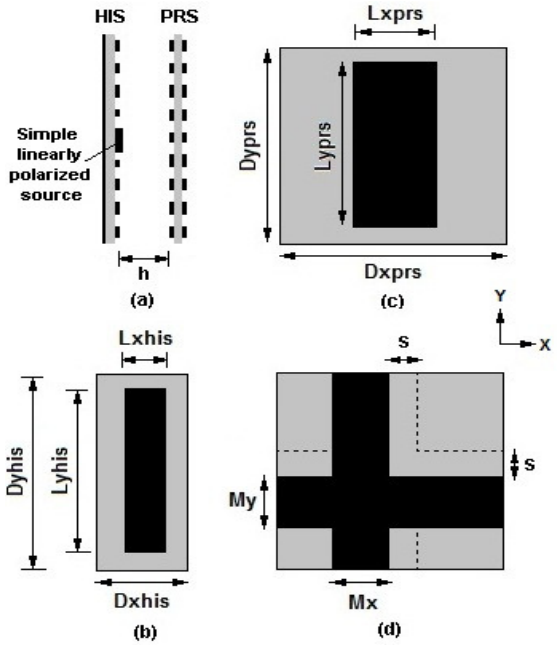

Fig. 1. Schematic layout of the proposed CP Fabry-Perot antenna a) Cavity antenna consisting of a high impedance surface (HIS) ground plane and a partially reflective surface (PRS) with excitation source. b) A unit cell of the HIS array. c) Top and d) bottom of a PRS array unit cell.

Various implementations of FP antennas have been reported in the literature, including PRSs made of bulk metal structures [1], [5]-[7] and stacks of dielectric slabs [9]-[11]. The use of Frequency Selective Surfaces (FSS) was introduced for the realization of the PRS in [4], benefiting from advantages associated with printed circuit board (PCB) technology. More recently, PCB arrays were introduced in the fully metalized ground plane to construct equivalent high impedance surfaces (HIS) [12], [13] that allow reduction of the profile of the FP cavity to sub-wavelength dimensions [14]-[15] and design flexibility with regard to the radiation properties [16]. Reduction of the cavity thickness has also been achieved by using a highly reflective double-layer PRS which also exhibits artificial magnetic conductor (AMC) properties [17].

While the aforementioned developments have established a relatively mature technology for low cost lightweight LP high gain antennas, they stop short of addressing applications that require circular polarization (CP) operation. When compared

Manuscript received February 3, 2013; revised June 2, 2013; accepted July 22, 2013. The work was supported by the Department of Employment and Learning (DEL) Northern Ireland.

R. Orr and V. Fusco are with the Institute of Electronics Communications and Information Technology, Queens University Belfast, Northern Ireland Science Park, Belfast, BT3 9DT, UK (e-mail: rorr08@qub.ac.uk, v.fusco@ecit.qub.ac.uk).

G. Goussetis was with the Institute of Electronics Communications and Information Technology, Queens University Belfast, BT3 9DT, UK. He is now partly with the same institutions and partly with the Institute of Sensors Signals and Systems, Heriot-Watt University, Edinburgh, EH14 4AS, UK (g.goussetis@ieee.org).

This article has been accepted for publication in a future issue of this journal, but has not been fully edited. Content may change prior to final publication. Citation information: DOI 10.1109/TAP.2013.2286839, IEEE Transactions on Antennas and Propagation

to LP, CP links benefit from resilience to reflections in multipath environments as well as other polarization dependent propagation effects (such as Faraday rotation [18] and reduction of rain clutter [19]), while also removing the requirement for polarization alignment between the transmitter and receiver. Such advantages are among the primary drives for the increasing use of CP in terrestrial [20], [21] and satellite [22] wireless links as well as imaging systems [23], [24].

A class of FP antennas proposed to address CP requirements is based on primary CP feeds [25], [26]. The latter commonly introduces increased complexity in the feeding network, hence partly undermining fabrication simplicity and cost-efficiency, particularly for applications in the mm-wave range and beyond. Another class of CP FP antennas relies on a LP primary source, typically aligned along slant 45° angle, and FP cavities made up of surfaces which are designed to provide conversion to CP [27]-[31].

An antenna concept that exploits an LP to CP transmission polarizer was proposed in [27], [28]. A purely metallic prototype consisting of three one-dimensional arrays placed above a metallic ground plane is reported, where two of the arrays act as a polarizer while the third acts as a PRS [27], [28]. The significant additional complexity associated with the three required layers, e.g. difficulty of alignment and poor return loss (>-2dB) was reported. In [29] it was proposed to exploit an asymmetric PRS operating at the 3 dB capacitive and inductive reflection point for each of the LP components respectively. Although this concept was demonstrated to produce CP, the antenna gain was limited by the 3dB reflection of the PRS [1]. This limitation was overcome in [30] by placing a two-layer FSS polarizing radome over a stacked FP cavity antenna. The stacked cavity antenna provides high gain while the polarizer converts LP to CP. However this comes at a cost of the increased fabrication complexity and profile associated with two stacked cavities and a two-layer polarizing radome.

In this paper a method of designing CP FP cavity antennas that overcomes the aforementioned limitations is proposed. The proposed antenna, schematically depicted in Fig. 1, consists of a single FP cavity and exploits a HIS and a double-sided PRS that allows independent control of the reflection/transmission magnitude and phase characteristics. The design concept along with a sensitivity analysis was presented in [32]. Here, a ray-optics model is introduced that allows producing an equation for the electric field in the cavity for a given plane wave far-field excitation. From this, design guidelines to obtain CP and high gain are derived. The concept is presented and validated by means of a design example and experimental validation.

II. Synthesis Technique

In [1] an equation is derived to give the electric field intensity in the Fraunhofer zone and the corresponding power pattern for Fabry-Perot antennas with a given primary source. Although this model is sufficiently accurate, it does not capture the electric field phase information, which is critical for CP operation. For this reason a modification of that model is presented here, which takes into account the standing wave effects between the PRS and the ground plane thus allowing an accurate estimation of the electric field (magnitude and phase) inside the cavity upon illumination of the antenna with a plane wave from the far-field. By comparatively studying the fields inside the cavity excited for two LP incoming waves oriented along the x- and y-axes respectively (Fig. 1) and invoking reciprocity [33]-[35], design guidelines for the PRS and HIS can then be obtained.

With reference to Fig. 2, consider a plane wave incident on a cavity made up of a HIS ground plane and a two layer PRS. A ray tracing approach is adopted where E_0, E_1, E_2, etc, are the electric fields associated with each of the numbered partial rays inside the cavity. Given the first-order mode approximation, the observation point is assumed to lie in the middle of the cavity, $z=h/2$ [35]. Following the approach of [1] we can write:

$$\begin{aligned} E_0 &= T_{PRS} e^{j({}^{T}\phi_{PRS} - \beta h/2)} \\ E_1 &= T_{PRS} R_{GP} e^{j({}^{T}\phi_{PRS} + {}^{R}\phi_{GP} - 3\beta h/2)} \\ E_2 &= T_{PRS} R_{PRS} R_{GP} e^{j({}^{T}\phi_{PRS} + {}^{R}\phi_{PRS} + {}^{R}\phi_{GP} - 5\beta h/2)} \\ E_3 &= T_{PRS} R_{PRS} R_{GP}^2 e^{j({}^{T}\phi_{PRS} + {}^{R}\phi_{PRS} + 2\,{}^{R}\phi_{GP} - 7\beta h/2)} \\ &\cdots \end{aligned} \quad (1)$$

where R_{PRS}/T_{PRS} and ${}^{R}\phi_{PRS}/{}^{T}\phi_{PRS}$ are the magnitude and phase of the PRS reflection/transmission coefficient and R_{GP} and ${}^{R}\phi_{GP}$ is the magnitude and phase of the HIS reflection coefficient.

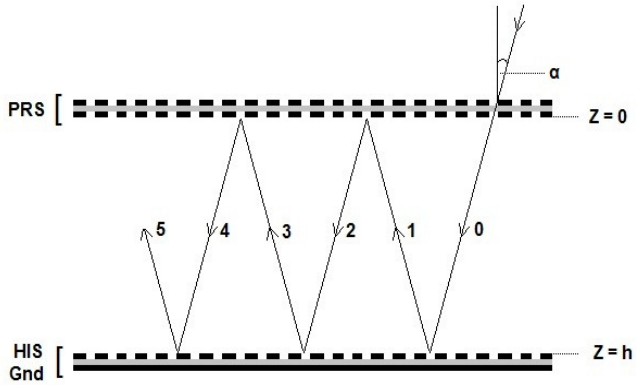

Fig. 2. Resonant cavity formed by a PRS and an AMC ground plane with excitation provided by a plane wave incident at an angle, α.

The electric field in the cavity can be obtained as the summation of the partial rays. The electric field related to the rays moving towards (even numbered) and away (odd numbered) from the HIS is represented by the equations below.

$$\begin{aligned} E_{EVEN} &= \sum_{n=0}^{\infty} T_{PRS} R_{PRS}^{n} R_{GP}^{n} e^{j({}^{T}\phi_{PRS} + \phi_n - \beta h/2)} \\ E_{ODD} &= \sum_{n=0}^{\infty} T_{PRS} R_{PRS}^{n} R_{GP}^{n+1} e^{j({}^{T}\phi_{PRS} + {}^{R}\phi_{GP} + \phi_n - 3\beta h/2)} \end{aligned}$$

where, $\phi_n = n\psi = n({}^{R}\phi_{PRS} + {}^{R}\phi_{GP} - 2\beta h)$. Given that $|R_{PRS} R_{GP}| < 1$, these equations can be simplified exploiting the infinite geometric series identity. Their sum will then give

This article has been accepted for publication in a future issue of this journal, but has not been fully edited. Content may change prior to final publication. Citation information: DOI 10.1109/TAP.2013.2286839, IEEE Transactions on Antennas and Propagation

the following expression for the total electric field in the cavity:

$$E = \frac{{}^{T}_{PRS}e^{j\,{}^{T}\phi_{PRS}}\left(e^{-j\beta h/2}+R_{GP}e^{j({}^{R}\phi_{GP}-3\beta h/2)}\right)}{1-R_{PRS}R_{GP}e^{j\psi}} \quad (2)$$

The above analysis applies to each of the two orthogonal LP components independently. The design objective can now be reduced to selecting the PRS and HIS responses for the two orthogonal LP components so that; a) the broadside directivity obtained for the two LP components is equal, and; b) a 90° phase difference between the two LP components is obtained at the observation point inside the cavity for a given excitation by a normally incident plane wave polarized at 45°. According to the theory of reciprocity achieving these two conditions would ensure that CP is produced in the far-field if excitation is provided inside the cavity by a linear source rotated by 45°.

Equation (2) has multiple degrees of freedom with respect to the unknown parameters. In order to study it further, it is instructive to impose some further assumptions. In particular, we first consider the lossless case, so that $R_{GP} = 1$ and $R_{PRS}^2 + T_{PRS}^2 = 1$ and that the resonance condition is met for both polarizations:

$${}^{R}_{X,Y}\phi_{PRS} + {}^{R}_{X,Y}\phi_{GP} - \frac{4\pi}{\lambda}h = \pm 2n\pi \quad n = 0,1,2 \ldots \quad (3)$$

where here and in the remaining the left-hand-side subscript refers to the polarization. Equation (2) then reduces to:

$$E = 2\sqrt{\frac{1+R_{PRS}}{1-R_{PRS}}}\cos\left(\frac{\beta h - {}^{R}\phi_{PRS}}{2}\right)e^{j({}^{T}\phi_{PRS} - {}^{R}\phi_{PRS}/2)} \quad (4)$$

For CP, the phase difference between the two LP components must be equal to an odd multiple of 90°. This gives the following condition for the phase $\Delta\theta$ defined in (5) below, which from this point onwards will be referred to as design phase:-

$$\Delta\theta = \left({}^{T}_{Y}\phi_{PRS} - \frac{{}^{R}_{Y}\phi_{PRS}}{2}\right) - \left({}^{T}_{X}\phi_{PRS} - \frac{{}^{R}_{X}\phi_{PRS}}{2}\right) = \pm n\frac{\pi}{2}$$
$$n = 1,3,5 \ldots \quad (5)$$

Commonly to this type of antennas, a LP primary source for the Fabry-Perot cavity is selected at the outset depending on implementation requirements. Assuming that the gain of the primary source is G_p and the antenna gain is G, then the directivity enhancement [4] provided by the Fabry-Perot cavity, G_r, for each LP component should be (in dB):

$$G_r = G - G_p \quad (6)$$

An equation derived in [4] gives an approximation of the directivity enhancement, G_r, provided by the Fabry-Perot cavity in terms of the magnitude of the PRS reflection coefficient, R_{PRS}, for each LP component,

$$G_r = \frac{1+R_{PRS}}{1-R_{PRS}} \quad (7)$$

Using (7) the required PRS reflectivity for each LP component, R_{PRS}, so that the antenna produces the desired gain, G, can be obtained. The main steps involved in the design of the antenna once the primary source has been selected are as below:

1. Starting from the desired gain, the directivity enhancement to be provided by the cavity to each LP component can be determined using (6). The PRS reflectivity for each LP component to provide this enhancement can be calculated from (7).
2. A PRS is designed which at the operating frequency provides for both LP components the reflection coefficient magnitude determined by equation (7) while the corresponding phases satisfy (5). The double-sided PRS unit cell shown in Fig. 1(c, d) provides a suitable geometry to achieve these conditions simultaneously. Initially the mesh array (Fig. 1d) which primarily determines the reflection magnitude is designed. Following this the dipole array (Fig. 1c) which primarily controls the transmission phase is designed. The PRS is then optimized to meet the required conditions.
3. An anisotropic HIS is subsequently designed to ensure that the resonance condition (3) is met for each orthogonal component.
4. The finite antenna is modeled and simulated. A minimal amount of optimization is required to achieve the desired performance.

III. Design Example

In this section, the design procedure outlined above is illustrated by means of an example involving an antenna operating at 15 GHz. The antenna is required to have a directivity of G = 21.5 dBi. The PRS for this (Fig. 1c, d) consists of a dielectric layer with a periodic metallic mesh array patterned on the bottom, which primarily controls the reflectivity for both polarizations (Fig. 1d), and a periodic metallic patch array patterned on the top (Fig. 1c), which primarily allows independent control of the transmission phase for the y-polarized waves. A relative shift, S, between the two arrays is allowed (Fig. 1d) for further design flexibility. Altering S mainly affects the transmission phase of the y-polarized waves. This PRS therefore allows meeting the design requirements for CP for an arbitrary antenna gain. Likewise, a suitable HIS for this antenna is depicted in Fig. 1b. It comprises a dipole array which allows control of the reflection phase of y-polarized waves. The HIS and PRS unit cells are commensurate to facilitate simulation [35].

In order to maintain simplicity, a microstrip patch is selected as the primary source for the antenna. A typical directivity of G_p = 6 dBi at 15 GHz is assumed for the patch. In order to provide a total directivity of G = 21.5 dBi the directivity enhancement to be provided by the Fabry-Perot cavity is therefore G_r = 15.5 dBi (6). According to (7), in order to provide this enhancement the PRS reflection coefficient magnitude should be equal to approximately R_{PRS} = -0.49 dB. A PRS unit cell has therefore been designed to

This article has been accepted for publication in a future issue of this journal, but has not been fully edited. Content may change prior to final publication. Citation information: DOI 10.1109/TAP.2013.2286839, IEEE Transactions on Antennas and Propagation

provide a reflection coefficient of R_{PRS} = -0.49 dB at 15 GHz for both LP components while also satisfying (5). A HIS unit cell (Fig. 1b) was then designed to ensure the resonance condition (3) was met for each polarization.

CST Microwave Studio was employed for the simulation and design of the PRS and HIS. A dielectric substrate with permittivity ε_r = 3, loss tangent tanδ = 0.003 and thickness of 1.14 mm was used. Conductors were assumed made of copper with thickness of 35 μm. In each case a unit cell of the periodic array was constructed and the y- and x-boundaries were set to unit cell implying that the structure was of infinite size in these directions. Floquet ports were set up at the z-boundaries. Metallic and dielectric losses were considered in the simulations. Parametric studies were carried out to achieve a PRS design which satisfied the identified requirements.

Referring to Fig. 1c and Fig. 1d the optimized dimensions are $D_{yprs} = D_{xprs}$ = 5.5 mm, L_{yprs} = 4.9 mm, L_{xprs} = 1 mm, $M_y = M_x$ = 2 mm and S = 0. Fig. 3 displays the simulated PRS reflection coefficient magnitude of the design for each polarization. The design phase, $\Delta\theta$ of equation (5), is also plotted.

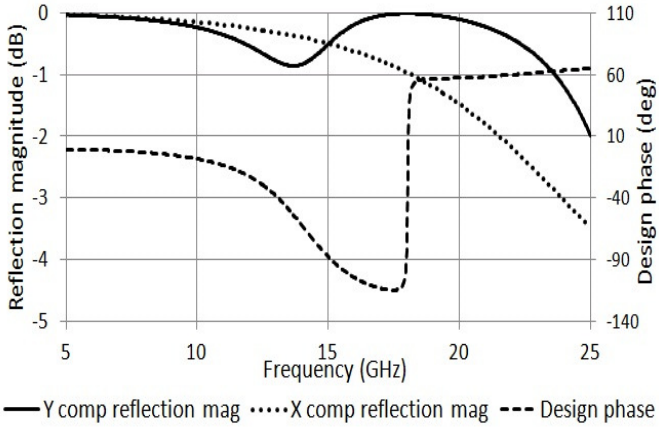

Fig. 3. Simulated reflection coefficient magnitude of two layer PRS (y- and x-components) and design phase.

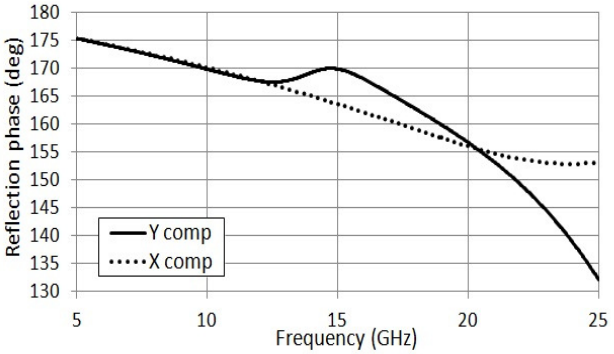

Fig. 4. Simulated reflection coefficient phase of two layer PRS (y- and x-components).

As shown in Fig. 3, the design conditions related to the PRS are to a good approximation satisfied at 15 GHz; the PRS reflection coefficient magnitude is approximately equal to -0.49 dB at 15 GHz for each orthogonal component and the design phase, which is required to be an odd multiple of 90°, is -88°. The phase of the reflection coefficient for this PRS is shown in Fig. 4. As shown, at 15 GHz the reflection phase is different for each orthogonal component; with reference to Fig. 1, the reflection phase for the y-component is 170° and for the x-component is 164° (Fig. 4). An anisotropic HIS ground plane is therefore required to compensate for this difference allowing the FP cavity resonance condition to be satisfied for each component. According to the above, the HIS should provide a reflection phase difference between the two LP components, ${}^{R}_{Y}\phi_{GP} - {}^{R}_{X}\phi_{GP}$= -6°.

The same dielectric material used for the PRS has been considered for the realization of the HIS. Referring to Fig. 1b the optimized dimensions are D_{yhis} = 5.5 mm, D_{xhis} = 1.1 mm, L_{yhis} = 2 mm and L_{xhis} = 0.6 mm. Fig. 5 displays the simulated HIS reflection phase for each orthogonal component as well as the phase difference between the two components. The reflection coefficient magnitudes for each component are approximately equal at 15 GHz and as displayed the reflection phase difference, ${}^{R}_{Y}\phi_{GP} - {}^{R}_{X}\phi_{GP} = -6°$ indicating that the design requirements for the HIS are met.

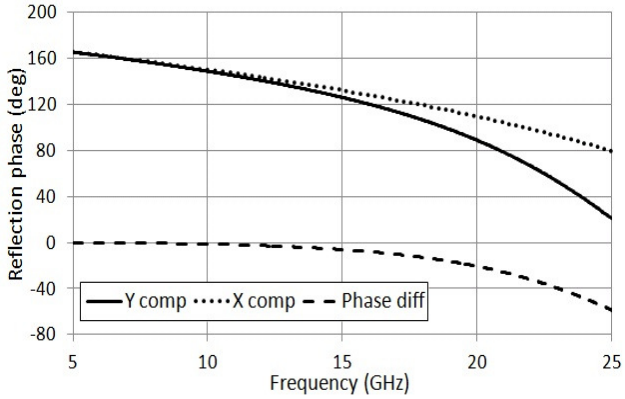

Fig. 5. Simulated reflection coefficient phase of high impedance surface ground plane – y- and x-components plus phase difference.

In order to verify (2), full-wave simulations to obtain the electric field in a single unit cell of the cavity upon LP plane wave incidence were carried out using CST MWS. The cavity height, *h*, was calculated from (3) to be 8.2 mm (≈ 0.4λ at 15 GHz). A unit cell of the PRS was placed at this height above 5 of the HIS unit cells. Electric and magnetic walls were set at the y- and x- boundaries. Illumination was provided by a normally incident plane wave with an Electric field vector of 1 V/m. An electric field probe at the center of the unit cell (x = 0, y = 0) and at the center of the cavity (z = h/2) detected each orthogonal field component. Displayed in Fig. 6 is the obtained electric field magnitude for both orthogonal components and the phase difference between the two components. Together the numerical results calculated using (2) and the simulated responses of the PRS and HIS are superimposed. There is good agreement between the calculated results and those obtained from simulations therefore validating the model proposed in section II.

Invoking reciprocity [33]-[35], these simulations can further provide estimation on the polarization of the radiation emitted from such an antenna. Within the remit of reciprocity arguments [33]-[35], the magnitude and phase of each radiated component is proportional to the magnitude and phase of the

This article has been accepted for publication in a future issue of this journal, but has not been fully edited. Content may change prior to final publication. Citation information: DOI 10.1109/TAP.2013.2286839, IEEE Transactions on Antennas and Propagation

corresponding field at the observation point. The simulation results show that maximum electric field occurs at 15 GHz for both components and the magnitudes are approximately equal. The simulated phase difference is -83°. The estimated axial ratio at 15 GHz from these results is approximately 1.3 dB. This result was not further optimized at this stage as there will be some discrepancies between this ideal model and the finite antenna simulation. The finite antenna will be optimized to achieve the desired result.

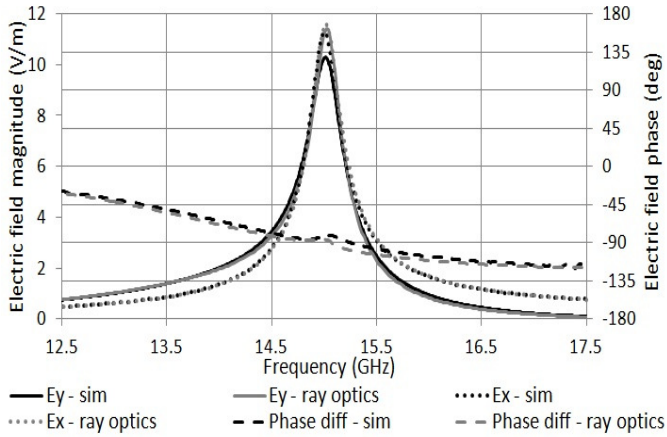

Fig. 6. Electric field magnitude (y- and x-components) plus Electric field phase difference from simulations and the ray optics model at the centre of the unit cell and the centre of the cavity (x=0, y=0, z=h/2).

IV. Experimental Results

A finite antenna was simulated using CST MWS. The antenna was formed by placing the PRS at the resonant distance h = 8.2 mm above the HIS ground plane as in Fig. 1a. PRS and HIS unit cell dimensions listed in section 3 were used in the simulation. The lateral size of the antenna was 137.5 x 137.5 mm^2 (approximately 7 x 7λ at 15 GHz) which equates to 25 x 25 PRS unit cells. This size was chosen to give a practical design with minimized edge effects. Further decreasing the antenna size degraded the radiation performance giving higher sidelobes and a lower directivity. Initial simulations were carried out using a simple center fed wire model dipole as a primary source to estimate the performance of the finite antenna. The dipole was located at the center of the antenna (x = 0, y = 0) and the center of the cavity (z = h/2). Magnetic and electric symmetry walls can be used to reduce the computational space to a quarter of the original, reducing the computational time of the simulation. The results are superimposed in Fig. 7 and are in good agreement with theoretical expectations. Maximum directivity is at 15.05 GHz. The axial ratio at this frequency is 1.5 dB.

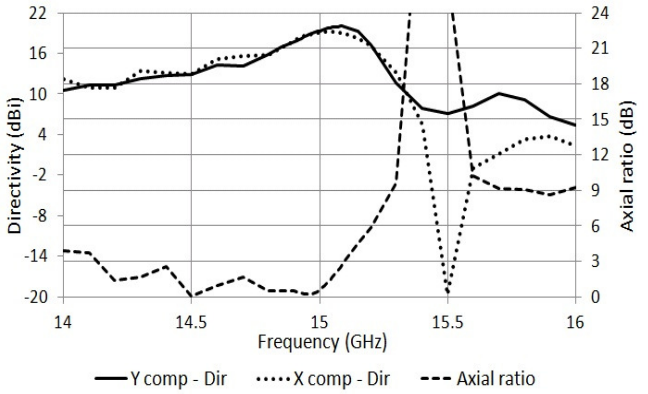

Fig. 7. Simulated directivity (y- and x-components) and axial ratio of finite antenna with simple dipole model source.

The designed PRS and HIS ground plane were fabricated and measured. In each case the array was photo-etched on a Taconic TLC-30 laminate. Standard-gain Ku-band horn antennas were used in the measurement of the complex transmission and reflection coefficient – one acting as the transmitter and the other the receiver. To measure transmission coefficient the LP horn antennas were connected to a Vector Network Analyzer (VNA) and placed on either side of the array. The antennas are placed at normal incidence and 106 cm from the array which is supported by a stand and surrounded by radar absorbing material (RAM). The complex transmission coefficient is measured using the horn antennas and then normalized with respect to an identical measurement where the array has been removed. To measure the complex reflection coefficient the horns were placed side by side at a small angle from the normal to the array. This measurement was normalized with the array replaced with a metallic plate of the same dimensions. Rotating the array by 90° gave Y and X components in each case. Fig. 8 compares the simulated and measured PRS reflection magnitude for each component. Also included is a comparison for the transmission phase difference.

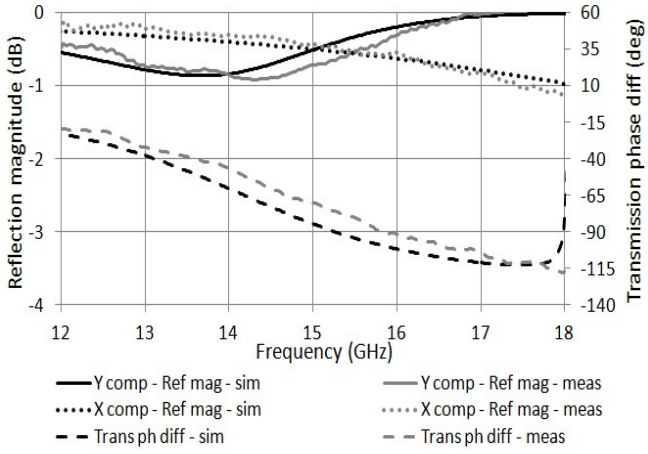

Fig. 8. Reflection magnitude (y- and x-components) and transmission phase difference of PRS – simulation and measurement

The agreement between simulation and measurement results was not as good as expected. In the simulated result the magnitude of reflection is equal for each component at

This article has been accepted for publication in a future issue of this journal, but has not been fully edited. Content may change prior to final publication. Citation information: DOI 10.1109/TAP.2013.2286839, IEEE Transactions on Antennas and Propagation

approximately 15 GHz while for the measured result is at 15.5 GHz. Furthermore simulated transmission phase difference at 15 GHz is -84° while measured is -70°. The discrepancy is primarily attributed to unwanted curvature of the PRS surface but also to uncertainty around the value of the relative permittivity and fabrication tolerances. The PRS design was therefore altered to achieve a measurement result with reflection magnitude equal for each component at 15 GHz. Fig. 9 compares the measurement results for the altered PRS with the simulation results of the original PRS with dimensions listed in Section 3. Nominal unit cell dimensions of the altered PRS are as follows: $D_{yprs} = D_{xprs} = 5.5$ mm, $L_{yprs} = 5$ mm, $L_{xprs} = 1$ mm, $M_y = M_x = 2$ mm and $S = 1.8$ mm. Substrate remained the same as for original design.

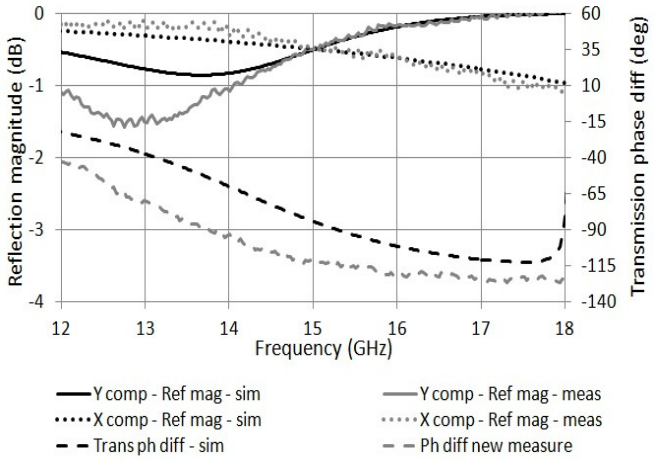

Fig. 9. Comparison between original PRS simulation and altered PRS measurement - reflection magnitude (y- and x-components) and transmission phase difference

At approximately 15 GHz reflection magnitude for each component is now equal. The simulated difference of the transmission phase for the two LP components at this frequency is -84° while measured is -114°. The differential reflection phase between the two LP components for the altered PRS was now 11° at 15 GHz. A new HIS was therefore designed with L_{yhis}= 2.3 mm to compensate for this increased phase difference. Other dimensions and substrate remained the same to those described in section III. The HIS was fabricated on the same substrate and attached to a flat solid surface to avoid curvature effects. Its reflection properties were measured using the technique described above. Fig. 10 shows the simulated and measured reflection coefficient phase for HIS with L_{yhis}= 2.3 mm. Good agreement between simulated and measured results is observed.

A realistic microstrip patch antenna was designed to feed the cavity. The antenna is printed on the dielectric substrate of the HIS. Five HIS unit cells were left out to allow for the copper patch. The patch is rotated by 45° with respect to the HIS dipoles to equally excite the x- and y-components of the electric field. A semi-rigid coaxial cable is used to feed the patch from underneath. The outer sheath and dielectric of the coaxial cable stop at the ground plane of the HIS while the inner conductor continues through the HIS substrate and connects to the patch. For correct operation, the patch size is 5 x 2.5 mm while to provide good matching it is fed 1mm off its center. The simulated directivity for the patch (not shown here for brevity) is found to be 6 dBi. From (3) the cavity height was calculated to be 8.2 mm. Following some full-wave optimization, the height was increased to 8.3 mm to ensure maximum directivity was at 15 GHz and to improve the axial ratio.

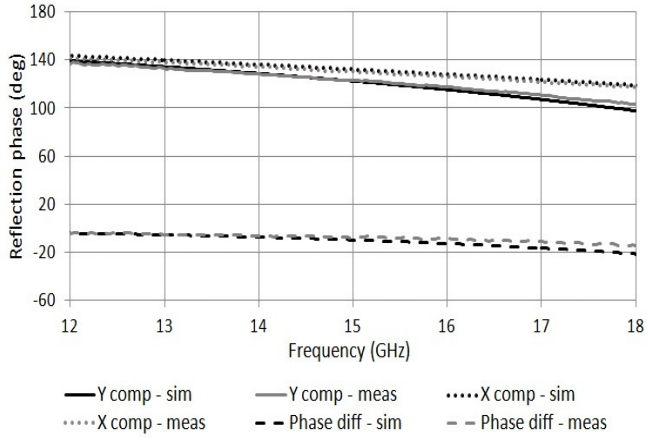

Fig. 10. Simulated and measured reflection phase (y- and x-components plus phase difference) of HIS with l_{yhis} = 2.3

(a)

(b)

Fig. 11. a) Assembled Fabry-Perot cavity antenna. b) Antenna with PRS removed. Inset shows microstrip patch antenna printed on HIS.

The antenna was assembled using the experimentally optimized PRS and the new HIS. Fig. 11a shows the assembled antenna while Fig. 11b shows the antenna with the PRS removed. The inset in Fig. 11b shows the patch antenna printed on the HIS ground plane. The measured cavity height

This article has been accepted for publication in a future issue of this journal, but has not been fully edited. Content may change prior to final publication. Citation information: DOI 10.1109/TAP.2013.2286839, IEEE Transactions on Antennas and Propagation

was 7.9 mm. Fig. 12 shows the realized gain of the antenna. There is good agreement between the simulated and measured results. Maximum simulated gain is 21.1 dB at 15 GHz while maximum measured gain is 19.1 dB at 15 GHz. The simulated directivity at 15 GHz was 21.7 dBi. There is good agreement between this and the value estimated using the equations derived from Ray Optics analysis (21.5 dBi).

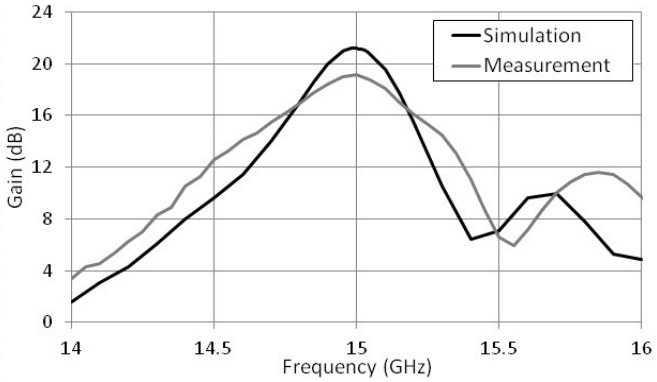

Fig. 12. Gain (simulated and measured) of finite antenna with a patch antenna source.

The measured antenna axial ratio and return loss are depicted in Fig. 13 and Fig. 14 respectively. The minimum simulated axial ratio is 0.46 dB at 14.96 GHz. At 15 GHz the simulated and measured axial ratio is approximately 0.6 dB. The simulated 3 dB axial ratio bandwidth is from 14.05 to 15.1 GHz (7%) while the measured 3 dB axial ratio bandwidth is from 13.8 to 15.2 (9%). The simulated 3 dB directivity bandwidth is from 14.8 to 15.15 GHz (2%) while the measured 3 dB directivity bandwidth is from 14.75 to 15.2 GHz (3%). The antenna operating bandwidth (intersection of the 3 dB axial ratio and directivity bandwidths) is therefore defined by the latter and from simulations is 2% while from measurements is 3%. This value is commensurate to the operating bandwidth of single cavity LP Fabry-Perot antennas [36]. At 15 GHz measured return loss is -15 dB. The radiation patterns were measured at 15 GHz for the two principal planes. Fig. 15 and Fig. 16 compare simulated and measured results. Good agreement between simulated and measurement results is observed. Highly directive patterns are achieved for both planes with sidelobe levels below -20 dB. Cross polarization level is less than -20 dB for each plane.

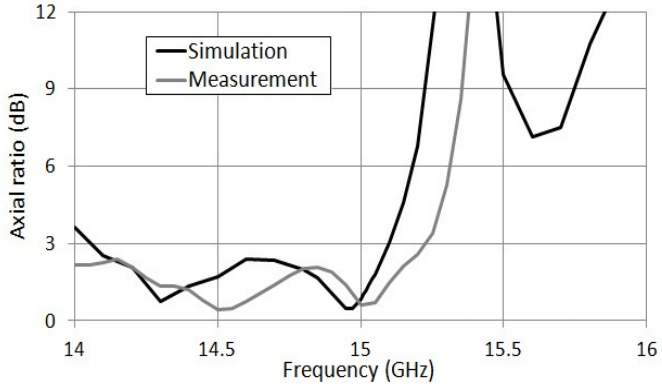

Fig. 13. Axial ratio (simulated and measured) of finite antenna with a patch antenna source.

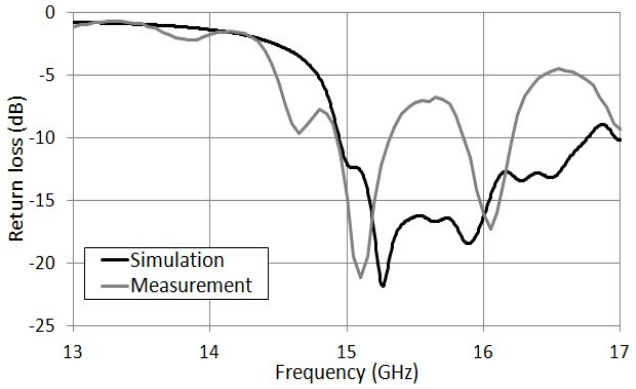

Fig. 14. Return loss (simulated and measured) of finite antenna with a patch antenna source.

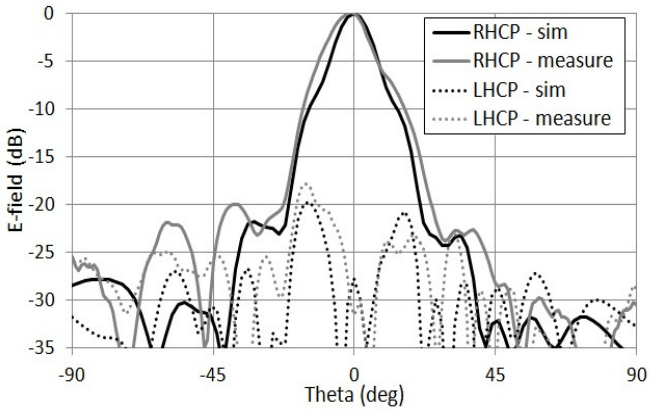

Fig. 15. Simulated and measured radiation patterns at 15 GHz, $\Phi = 0°$.

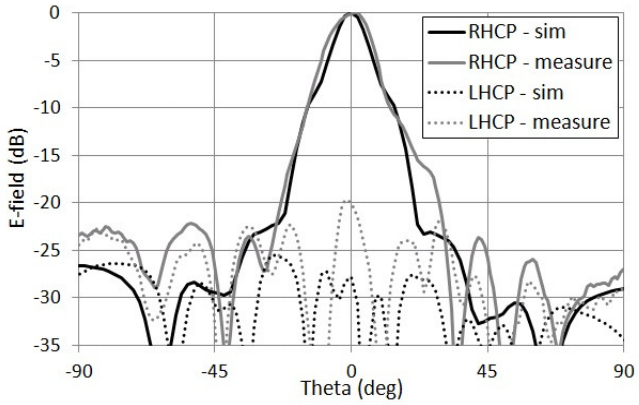

Fig. 16. Simulated and measured radiation patterns at 15 GHz, $\Phi = 90°$.

V. CONCLUSION

A method for producing a circularly polarized Fabry-Perot cavity antenna with arbitrary gain and a single cavity has been presented. The antenna exploits a double-sided PRS placed above an anisotropic HIS ground plane. The structure is appealing due to fabrication simplicity – single cavity with excitation provided by a linearly polarized source rotated by 45°. A simple ray-optics model is presented, which in conjunction with reciprocity provides an accurate design method for the antenna. A prototype antenna was designed to

validate the technique. Full-wave simulation results showed 21.1 dB at 15 GHz for this example. Measurements on a fabricated prototype agree well with this prediction.

ACKNOWLEDGMENT

The authors would like to thank G. Rafferty (Queen's University Belfast) for the fabrication of the arrays and Taconic Advanced Dielectric Division for providing the substrates.

REFERENCES

[1] G. V. Trentini, "Partially reflecting sheet array", *IRE Trans. Antennas Propag.,* vol. AP-4, pp. 666-671, 1956.

[2] J.R. James, S.J.A. Kinany, P.D. Peel, and G. Andrasic, "Leaky-wave multiple dichroic beamformers", *Electron. Lett*., 1989, 25, pp. 1209-1211.

[3] M. Thèvenot, C. Cheype, A. Reineix, and B. Jecko, "Directive photonic band-gap antennas," *IEEE Trans. Microw. Theory Tech.,* vol. 47, no. 11, pp. 2115-2122, Nov. 1999

[4] A. P. Feresidis, and J. C. Vardaxoglou, "High-gain planar antenna using optimized partially reflective surfaces," *IEE Proc. Microw. Antennas Propag*., vol. 148, no. 6, Feb. 2001.

[5] R. Sauleau, Ph. Coquet, T. Matsui, and J.-P. Daniel, "A new concept of focusing antennas using plane-parallel Fabry-Perot cavities with non-uniform mirrors," *IEEE Trans. Antennas Propag.*, vol. 51, no. 11, pp. 3171-3175, Nov. 2003.

[6] N. Guérin, S. Enoch, G. Tayeb, P. Sabouroux, P. Vincent, and H. Legay, "A metallic Fabry Perot directive antenna," *IEEE Trans. Antennas Propag*., vol. 54, no. 1, pp. 220-224, Jan. 2006.

[7] O. Roncière, B. A. Arcos, R. Sauleau, K. Mahdjoubi, and H. Legay, "Radiation performance of purely metallic waveguide fed compact Fabry Perot antennas for space applications," *Microw. Opt. Tech. Lett.,* vol. 49, Sep. 2007, pp. 2216-2221.

[8] A. P. Feresidis, G. Goussetis, and J. C. Vardaxoglou, "A broadband high gain resonant cavity antenna with single feed," *1st European Conference on Antennas and Propagation, EuCAP,* Nice, France, pp. 1-5, Nov. 2006.

[9] D.R. Jackson, and N. G. Alexopoulos, "Gain enhancement methods for printed-circuit antennas," *IEEE Trans. Antennas Propag*., vol. 33, pp. 976-987, 1985.

[10] R. Gardelli, M. Albani, and F. Capolino, "Array thinning by using antennas in a Fabry-Perot cavity for gain enhancement," *IEEE Trans. Antennas Propag.,* vol. 54, no. 7, pp. 1979–90, Jul. 2006.

[11] C. Cheype, C. Serier, M. Thevenot, T. Monediere, A. Reineix, and B. Jecko, "An electromagnetic band gap resonator antenna," *IEEE Trans. Antennas Propag*., vol. 50, no. 9, pp. 1285-1290, 2002.

[12] D. Sievenpiper, Z. Lijun, R. F. Broas, N. G. Alexopoulos, and E. Yablonovitch, "High-impedance electromagnetic surfaces with a forbidden frequency band," *IEEE Trans. Microw. Theory Tech.,* vol. 47, no. 11, pp. 2059-2074, Nov. 1999.

[13] Y. Zhang, J. von Younis, C. Fischer, and W. Wiesbeck, "Planar artificial magnetic conductors and patch antennas," *IEEE Trans. Antennas Propag., Special Issue on Metamaterials,* vol. 51, no. 10, pp. 2704-2712, Oct. 2003.

[14] S. Wang, A. P. Feresidis, G. Goussetis, and J.C. Vardaxoglou, "Low-profile resonant cavity antenna with artificial magnetic conductor ground plane," *Electronics Letters*, vol. 40, no. 7, pp. 405-406, April 2004.

[15] A. P. Feresidis, G. Goussetis, S. Wang, and J. C. Vardaxoglou, "Artificial Magnetic Conductor Surfaces and Their Application to Low-Profile High- Gain Planar Antennas," *IEEE Trans. Antennas Propag.*, vol. 53, no. 1, pp. 209-215, Jan. 2005.

[16] M. Garcia-Vigueras, J.L. Gomez-Tornero, G. Goussetis, A. R. Weily, Y. J. Guo, "1D-Leaky Wave Antenna Employing Parallel-Plate Waveguide Loaded with PRS and HIS," *IEEE Transactions on Antennas and Propagation*, Vol. 59, No. 10, pp. 3687-3694, Oct. 2011.

[17] A. Ourir, A. de Lustrac, and J.-M. Lourtioz, "All-metamaterial-based subwavelength cavities (λ/60) for ultrathin directive antennas," *Applied Physics Lett.,* vol. 88, no. 8, pp. 84103-1-3, Feb. 2006.

[18] G. Maral and M. Bousquet, *Satellite Communications Systems: Systems, Techniques and Technology.* Sussex, U.K.: Wiley, 2009, ch. 5, p. 208.

[19] F. E. Nathanson, J. P. Reilly, and M. N. Cohen, *Radar Design Principles: Signal Processing and the Environment, Second edition.* Mendham, N.J., U.S.A.: SciTech Publishing, 1999, ch. 6, p. 231.

[20] A. R. Weily, and Y. Jay Guo, "Circularly polarized ellipse-loaded circular slot array for millimeter-wave WPAN applications," *IEEE Trans. Antennas Propag,* vol. 57, no. 10, pp. 2862-2870, Oct. 2009.

[21] J.-F. Zürcher, "A meander-line polarizer covering the full E-band," *Microw. Opt. Tech. Lett.,* vol. 18, Aug. 1998, pp. 320-323.

[22] M. Albani et al., "Concepts for Polarising Sheets and "Dual-gridded" Reflectors for Circular Polarisation," *ICECom Conference Proceedings,* Dubrovnik, Croatia, pp. 1-4, Sep. 2010.

[23] E. N. Grossman, A. Luukanen, and A. J. Miller, "Terahertz active directdetection imagers," *Proc. SPIE,* vol. 5411, pp. 68-77, Sep. 2004.

[24] C. Dietlein, A. Luukanen, Z. B. Popovic, and E. Grossman, "A W-band polarization converter and isolator," *IEEE Trans. Antennas Propag.,* vol. 55, no. 6, pp. 1804-1809, Jun. 2007.

[25] A.R. Weily et al., "High gain circularly polarized 1-D EBG resonator antenna," *Electron. Lett.,* vol. *42, no. 18, Aug. 2006, pp. 10*12-1013.

[26] D.H. Lee et al., "Directive enhancem*e*nt of circular polarized patch antenna using ring-shaped frequency selective surface superstrate," *Microw. Opt. Tech. Lett.,* vol. 49, Jan. 2007, pp. 199-201.

[27] M. Diblanc, E. Rodes, E. Arnaud, M. Thèvenot, Th. Monédière, and B. Jecko, "Circularly polarized metallic EBG antenna," *IEEE Microwave Wireless Comp. Lett.,* vol. 15, no.10, pp. 638-640, Oct. 2005.

[28] E. Arnaud, R. Chantalat, M. Koubeissi, T. Monédière, M. Thèvenot, and B. Jecko, "Improved self polarizing metallic EBG antenna," *3rd European Conference on Antennas and Propagation, EuCAP 2009,* Berlin, Germany, pp. 3813-3817, Mar. 2009.

[29] S. A. Muhammad, R. Sauleau, and H. Legay, "Self generation of circular polarization using compact Fabry-Perot antennas," *IEEE Antenna Wireless Propag. Lett.,* vol. 10, pp. 907-910, 2011.

[30] S. A. Muhammad, R. Sauleau, and H. Legay, "Purely metallic waveguide-fed Fabry-Perot cavity antenna with a polarizing frequency selective surface for compact solutions in circular polarization," *IEEE Antenna Wireless Propag. Lett.,* vol. 11, pp. 881-884, 2012.

[31] J. Ju, D. Kim, W. Lee, and J. Choi, "Design Method of a Circularly-Polarized Antenna Using Fabry-Pérot Cavity Structure," *ETRI Journal*, vol.33, no.2, Apr. 2011, pp.163-168

[32] R. Orr, G. Goussetis, and V. Fusco, "Design of circularly polarized Fabry-Perot cavity antenna," *6th European Conference on Antennas and Propagation, EuCAP 2012,* Prague, Czech Republic, pp. 2716-2720, Mar. 2012.

[33] T. Zhao, D.R. Jackson, J.T. Williams, H.-Y.D. Yang, A.A. Oliner, "2-D periodic leaky-wave antennas-part I: metal patch design," *IEEE Trans. Antennas Propag*., vol.53, no.11, pp. 3505-3514, Nov. 2005.

[34] T. Zhao, D.R. Jackson, J.T. Williams, "2-D periodic leaky-wave Antennas-part II: slot design," *IEEE Trans. Antennas Propag*., vol.53, no.11, pp. 3515-3524, Nov. 2005.

[35] C. Mateo-Segura, G. Goussetis, A.P. Feresidis, "Sub-wavelength profile 2-D Leaky-wave antennas with two periodic layers," *IEEE Trans. Antennas Propag*., vol.59, no.2, pp. 416-424, Feb. 2011.

[36] C. Mateo-Segura, A. P. Feresidis, and G. Goussetis, "Bandwidth Enhancement of 2-D Leaky-Wave Antennas Using Double-Layer Periodic Surfaces," *IEEE Transactions Antennas and Propagation, submitted.*

Robert Orr received the M.Eng. (Hons.) degree in electrical and electronic engineering from The Queen's University of Belfast (QUB), Belfast, U.K., in 2009, and is currently pursuing the Ph.D. degree in high-frequency electronic circuits and antenna technologies at The Institute of Electronics, Communications and Information Technology (ECIT), QUB.

This article has been accepted for publication in a future issue of this journal, but has not been fully edited. Content may change prior to final publication. Citation information: DOI 10.1109/TAP.2013.2286839, IEEE Transactions on Antennas and Propagation

George Goussetis (S 99, M 02, SM 12) received the Diploma degree in Electrical and Computer Engineering from the National Technical University of Athens, Greece, in 1998, and the Ph.D. degree from the University of Westminster, London, UK, in 2002. In 2002 he also graduated B.Sc. in physics (first class) from University College London (UCL), UK.

In 1998, he joined the Space Engineering, Rome, Italy, as RF Engineer and in 1999 the Wireless Communications Research Group, University of Westminster, UK, as a Research Assistant. Between 2002 and 2006 he was a Senior Research Fellow at Loughborough University, UK. He was a Lecturer (Assistant Professor) with Heriot-Watt University, Edinburgh, UK between 2006 and 2009 and a Reader (Associate Professor) with Queen's University Belfast, UK, between 2009 and 2013. In 2013 he joined Heriot-Watt as a Reader. He has authored or co-authored over 150 peer-reviewed papers three book chapters and two patents. His research interests include the modelling and design of microwave filters, frequency-selective surfaces and periodic structures, leaky wave antennas, microwave sensing and curing as well numerical techniques for electromagnetics.

Dr. Goussetis has held a research fellowship from the Onassis foundation in 2001, a research fellowship from the UK Royal Academy of Engineering between 2006-2011 and a European Marie-Curie experienced researcher fellowship in 2011-12. In 2010 he was visiting Professor in UPCT, Spain. He is the co-recipient of the 2011 European Space Agency young engineer of the year prize, the 2011 EuCAP best student paper prize and the 2012 EuCAP best antenna theory paper prize.

Vincent F. Fusco (S'82–M'82–SM'96–F'04) received the Bachelor's degree (1st class honors) in electrical and electronic engineering, the Ph.D. degree in microwave electronics, and the D.Sc. degree, for his work on advanced front end architectures with enhanced functionality, from The Queens University of Belfast (QUB), Belfast, Northern Ireland, in 1979, 1982, and 2000, respectively.

He is head of the High Frequency Laboratories at QUB where he is also Director of the International Centre for Research for System on Chip and Advanced MicroWireless Integration (SoCaM). His research interests include active antenna and front-end MMIC techniques. He has published over 420 scientific papers in major journals and international conferences, and is the author of two textbooks. He holds patents related to self-tracking antennas and has contributed invited chapters to books in the fields of active antenna design and electromagnetic-field computation.

Prof. Fusco is a Fellow of both the Institution of Engineering and Technology and Institution of Electrical Engineers (U.K.). In addition he is a Fellow of the Royal Academy of Engineering and a member of the Royal Irish Academy. In 1986, he was awarded a British Telecommunications Fellowship and in 1997 he was awarded the NI Engineering Federation Trophy for outstanding industrially relevant research.